Research Article

Nano Research
2019, 12(8): 1862–1870

ISSN 1998-0124 CN 11-5974/O4
https://doi.org/10.1007/s12274-019-2449-x

Amine-rich carbon nitride nanoparticles: Synthesis, covalent functionalization with proteins and application in a fluorescence quenching assay

Gabriele Capilli†, Simone Cavalera, Laura Anfossi (✉), Cristina Giovannoli, Marco Minella (✉), Claudio Baggiani, and Claudio Minero

Department of Chemistry and NIS Center of Excellence, University of Torino, 10125 Torino, Italy
† Present address: Mining & Materials Engineering, McGill University, Montreal, Quebec H3A 0C5, Canada

Received: 20 December 2018 / **Revised:** 28 May 2019 / **Accepted:** 30 May 2019

ABSTRACT

Carbon nitride nanoparticles (CNNPs) have been employed as fluorescent sensing tools owing to their unique features, e.g. low cost production, high stability in water and high photoluminescence quantum yield. Here, an easy and versatile synthetic approach was exploited to design fluorescent nanoparticles with surface functionalities suitable for covalent binding to bioligands. High hydrophilic, brightly fluorescent CNNPs, rich of superficial amines, were obtained from the thermal condensation of urea and lysine ($CNNP^{Lys}$) and by tuning the precursor ratio and the heating time. Structure and size of the functionalized nanoparticles were characterized through infrared (IR) spectroscopy, transmission electron microscopy (TEM) and dynamic light scattering (DLS). Their optical properties were studied by ultraviolet–visible (UV–Vis) and fluorescence spectroscopy. The superficial primary amino groups, furnished by the lysine co-precursor, enabled for covalently linking $CNNP^{Lys}$ to model proteins. The $CNNP^{Lys}$-protein conjugates excited under UV irradiation emit in the 400–450 nm visible range (quantum yield 24%). The applicability of $CNNP^{Lys}$ as novel fluorescent probes was demonstrated by a fluorescence quenching assay, in which gold nanoparticles (GNPs) were attached to Staphylococcal protein A and employed to quench the $CNNP^{Lys}$ fluorescence by Forster resonant energy transfer (FRET). The quenching occurred upon formation of the specific binding between the GNP-linked protein A and $CNNP^{Lys}$-tagged immunoglobulins, while the inhibition of the binding resulted in the recovery of $CNNP^{Lys}$ luminescence. The synthetic strategy, based on combining a "conjugated polymer"-forming unit (urea) and a co-precursor able to provide the desired functional group (lysine), allows designing innovative materials for the development of new generation fluorescence biosensors in which easily functionalized fluorophores are needed.

KEYWORDS

fluorescent probe, carbon nitride nanoparticles, quenching assay, fluorescent materials, g-C_3N_4, Forster resonant energy transfer (FRET)

1 Introduction

Biosensors based on fluorescence detection have attained especial interest due to their high sensitivity and selectivity. The incorporation of fluorescent nanomaterials [1] and conjugated polymers [2] is regarded as a favorite route towards the development of a new class of high sensitive and selective tools for sensing of biomolecules.

Traditionally, fluorescent probes used as labels for bioanalysis are organic dyes and protein-based fluorophores, which suffer from serious chemical and photophysical liabilities, such as pH dependence, susceptibility to photo-bleaching, short-term stability in aqueous media and short lifetimes of the excited states [3]. These limitations have been partially overcome by using inorganic semiconductor quantum dots (QDs). However, these are toxic and suffer of low water compatibility and lack of functional groups available for the conjugation to biomolecules [4–8]. Carbon-based fluorescent nanomaterials are a safer and cost-effective alternative to inorganic QDs [9–12] while preserving excellent optical properties and chemical stability [9–11, 13].

C-based nanomaterials are becoming popular as fluorescent probes for analytical applications [14, 15], and especially bioimaging [10, 12, 16]. Carbon quantum dots (CQDs) [16, 17], graphene quantum dots (GQDs) [18] and carbon nanoparticles (CNPs) [12] are parts of this class of nanomaterials.

The main weakness of undoped carbon-based materials is the high photoluminescence self-quenching, which decreases the overall emission quantum yield (QY) [19]. In order to limit this undesired feature while preserving the positive properties, the research has focused on doping carbon nanomaterials with non-metallic heteroatoms, i.e. nitrogen, sulphur, oxygen and boron [20–22]. Graphitic carbon nitride (g-CN) nanomaterials in the form of nanosheets (g-CNNSs) [23–25], quantum dots (g-CNQDs) [26–28] and carbon nitride nanoparticles (CNNPs) [29, 30] are examples of N-rich carbon-based structures.

g-CN nanomaterials own a unique layered and π-conjugated structure composed by heptazine units bridged by amino groups [31]. The incorporation of N atoms in the carbon structure generates a combination of new relevant features. Above all, g-CN materials show a semiconducting behavior [32], a bright blue photoluminescence (PL) [24, 27] and the tunability of the optical properties (i.e. λ_{MAX} of emission) through the modification of both the graphene-like structure [28, 33, 34] and of the particle size. Most importantly, g-CN nanomaterials are water-soluble and intrinsically exhibit superficial functional groups. These have been exploited as sensing systems for

Address correspondence to Laura Anfossi, laura.anfossi@unito.it; Marco Minella, marco.minella@unito.it

the detection of metal ions [2, 14, 35–37]. The sensing mechanism is based on the fluorescence quenching due to the metal–g-CN binding formation. The selective detection is achieved through the metal interaction with the functional groups on the g-CN surface. The quenching of g-CN photoluminescence by Forster resonant energy transfer (FRET) has been also exploited for the sensitive detection of riboflavin, whose absorption overlaps the fluorescent probe emission [38].

However, the application of such materials for sensing is confined to charged analytes and to compounds with high affinity towards the typical surface groups of the g-CN structure. A tremendous advance for their wider application is represented by the possibility to exploit native superficial groups for the covalent binding of the g-CN fluorescent probes to bioreceptors and the incorporation of such nanomaterials into bioanalytical platforms based on the molecular recognition mechanisms (e.g. as probes for immunoassays or for biosensors). To this aim, the optimal probe should (i) be highly water-soluble and rich of functional groups available for the conjugation to biomolecules via consolidated protocols, (ii) preserve its optical properties (especially high QY) after the bioconjugation. Additional preferred features are the easy and cost-effective preparation and the tunability of the chemical functionalities.

Among g-CN nanomaterials, CNNPs, although showing photoluminescence QY often lower than g-CNNSs and g-CNQDs, are characterized by a definitely larger hydrophilicity and by the native presence of surface reactive groups [28, 29]. Moreover, CNNPs allow for controlling the nature and abundance of superficial functional groups, and the photoluminescence properties—which are strongly related to their surface states [13, 28]—by modifying the synthetic parameters, e.g. the precursors and the condensation time employed.

The CNNPs can be easily prepared through the so-called bottom-up and top-down syntheses [13, 39]. The former involves the condensation at high temperature of small nitrogen-rich organic molecules (i.e. urea [40], dicyandiamide [35], melamine [41], formamide [14], organic amines [30, 36] and so on) via microwave [14, 26], solvothermal [29] or solid thermal treatment [22, 28]. This approach requires a quite complex work-up of the reaction mixture to separate the CNNPs from the unreacted precursors [39]. Conversely, the top-down methods start from bulk g-CN and gives g-CNNSs and g-CNQDs by cutting and exfoliating the conjugated and strongly stacked aromatic planes via ultrasonic liquid exfoliation [24] and harsh processing (e.g. chemical oxidation with strong acids [35] or alkali [27, 42]). These techniques usually require longer procedures and the use of hazardous concentrated corrosive reactants. Typically, the process produces blue-fluorescent and hydrophilic CNNPs, owning some functional groups (hydroxy-, carboxy-, and amino-groups), resulting from the incomplete condensation of the precursors [43]. However, as far as we know, fluorescent CNNPs have never been used to label bioligands through covalent conjugation of their superficial functional groups.

In this work, we prepared a new fluorescent probe with the CNNP structure and rich of primary amino-groups available for their conjugation to bioligands. To attain the desired functional moieties, CNNPs have been synthesized using urea as "conjugated polymer"-forming monomer and lysine as a primary amino group-rich co-precursor.

We followed a facile, one-pot and cost effective synthetic route and optimized the synthetic parameters to reach bright fluorescence, good hydrophilicity and, above all, availability of primary amino-groups.

Physico-chemical and spectroscopic properties of the novel CNNPs were investigated by means of infrared (IR) spectroscopy, transmission electron microscopy (TEM), ultraviolet–visible (UV–Vis) absorption, fluorescence spectroscopy, and dynamic light scattering (DLS). The availability of superficial primary amines allowing for the conjugation of the CNNPs to biomolecules was confirmed by linking them to model proteins. Interestingly, we observed that the chemical modification of CNNPs, due to their conjugation to proteins, did not affect their optical properties. Therefore, we prepared a probe—comprising CNNPs as the fluorescent moiety and immunoglobulins as a model bioligand—and employed it to set up a fluorescence quenching assay (based on the FRET [44]) to detect human immunoglobulins G (IgG). FRET-based quenching assays are largely employed for biosensing thanks to their simplicity, specificity and sensitivity [25, 38]. Briefly, the fluorescent probe and the quencher are covalently linked to a receptor and to its ligand, respectively. Then the ligand-receptor specific interaction brings the quencher and the probe into close proximity, resulting in the fluorescence quenching. Then, the PL of the probe is modulated by the rate of the ligand-receptor complex formation. In this work, we linked rabbit immunoglobulins to the new amino-rich CNNPs and Staphylococcal protein A to gold nanoparticles, which acted as the fluorescent probe and the quencher, respectively. According to the assay principle, the PL of CNNPs linked to immunoglobulins was efficiently turned-off by the quencher and specifically recovered upon addition of free human IgG, thus demonstrating that the proposed approach enables for the production of excellent probes, which can be used for the development of new generation of fluorescence biosensors.

2 Experimental

2.1 Chemicals and materials

Urea (U), citric acid (Cit), lysine hydrochloride (Lys), glutaraldehyde, bovine serum albumin (BSA), tetrachloroauric acid, trisodium citrate, disodium monohydrogen phosphate dihydrate, sodium dihydrogen phosphate monohydrate, dichloromethane (DCM), Bradford Brilliant Blue Coomassie, Staphylococcus Aureus Protein A (SpA), rabbit and human immunoglobulins G (IgG) were purchased from Merck and Sigma Aldrich. All the chemicals were used without any further purification. Water was purified with a Milli-Q plus apparatus (total organic carbon (TOC) = 2 ppb, resistivity 18.2 MΩ·cm).

2.2 Synthesis of amine-rich CNNPs

Solid urea and lysine hydrochloride were mixed, in different molar ratio (U:Lys), namely 0:1, 1:1, 3:1, 6:1, 12:1, and 1:0. The amount of Lys was kept constant (3 mmol, 0.548 g). The solid mixture was grinded to uniform powder, then heated at 200 °C, in a sealed 100 mL Teflon-lined autoclave, for 2 to 16 h, and finally let to naturally cool down to room temperature. The resulting brownish-to-black, viscous-to-solid product was dissolved in water (50 mL in an ultrasonic bath (10 min)), filtered through a 0.45 μm Teflon membrane to remove the insoluble carbonized fraction, and stored at room temperature in the dark. The obtained suspensions were stable for months even under ambient light. Their spectroscopic features remained unvaried during the experiments. This demonstrated the high chemical stability of the new materials and their resistance to photobleaching in water [45].

The best material, selected as a compromise between bright fluorescence and good water solubility, was refined by washing three times with DCM (1:1 CNNP water solution:DCM).

A control material was prepared from a solid mixture of U and citric acid using 3:1 molar ratio and 2-h heating ($CNNP^{Cit}$), as described in Ref. [33].

2.3 Characterization of CNNPs

The fraction of condensed products dissolved in water (CNNPs) was gravimetrically quantified by freeze drying 1 mL of the solution and weighting the solid residue. The pH of CNNPs was roughly estimated by a universal pH indicator paper.

The ATR/FT-IR spectra were recorded with a PerkinElmer Spectrum Two UATR Spectrometer equipped with a diamond window. The spectra were acquired with a resolution of 1 cm^{-1} with 16 scans, on the solid materials obtained by freeze-drying the aqueous solutions.

High-resolution TEM (HR-TEM) were carried out on a JEOL JEM 3010UHR (300 kV) TEM Tokyo, Japan, fitted with a single crystal LaB_6 filament. Samples were dried deposited on Cu "holey" carbon grids (200 mesh).

DLS measurements were carried out using a Cilas Nano DS analyser (Orléans, France), equipped with a 638 nm diode laser and a temperature control (25 °C). The scattered laser fluctuation was detected at an angle of 60°. Hydrodynamic diameters were calculated by analyzing the autocorrelation functions with the Contin algorithm.

UV–Vis absorption and fluorescence characterizations were obtained by means of a Varian CARY 100 UV–Vis spectrophotometer (Agilent, CA, USA) and a Varian Cary Eclipse Fluorescence Spectrophotometer (Agilent, CA, USA), respectively.

In order to quantify the N/C molar ratio, the TOC and total organic nitrogen (TON) content were measured on diluted solutions of CNNPs (20 and 10 $mg{\cdot}L^{-1}$) through a Shimadzu ON-LINE TOC-VCSH instrument, equipped with an ASI-V autosampler and fed with zero-grade air (Gruppo Sapio, Italy).

2.4 Preparation of $CNNP^{Lys}$ bioconjugates

The bioconjugation of $CNNP^{Lys}$ with BSA ($CNNP^{Lys}$–BSA) was obtained by mixing 500 µL of 1.5 $mg{\cdot}mL^{-1}$ aqueous solution of $CNNP^{Lys}$, 50 µL of BSA (1% w/v in phosphate buffer 20 mM, pH 7.4, PB) and 9.4 µL of glutaraldehyde (25% in water). As a control, the same synthetic protocol was used to conjugate BSA to $CNNP^{Cit}$. The mixtures reacted overnight at room temperature under magnetic stirring. BSA-linked and unconjugated CNNPs were separated by size-exclusion chromatography (SEC) on a Sephadex G75 cartridge (GE Healthcare, IL, USA), using PB (with 0.13 M NaCl added) as the eluent. Eluates were separately collected in 1-mL fractions. Fractions containing CNNPs were detected by measuring the fluorescence emission with a microplate fluorescence reader (FLx800 from BioTek, VT, USA) (excitation filter 340 ± 15 nm, emission filter 420 ± 25 nm) for both materials. Fractions containing the protein were identified by staining with Comassie Brilliant Blue [46] and measuring the absorption at 595 nm by a microplate reader (Multiskan, ThermoFisher Scientific, PA, USA).

The same synthetic protocol was used to bioconjugate $CNNP^{Lys}$ with immunoglobulins ($CNNP^{Lys}$–IgG), with the following minor modifications: 136 µL of rabbit IgG (1% w/v in PB) were used instead of BSA, and the particulate matter formed during the conjugation was removed by centrifugation at 2,400*g* for 15 min before separation via SEC.

2.5 Preparation of the quencher

The synthesis of the gold nanoparticles (GNPs) and the adsorption of SpA onto GNPs (GNP–SpA) were carried out as previously described [47]. GNPs were obtained by citrate reduction of tetrachloroauric acid [48]. Then, SpA was passively adsorbed onto GNPs and the uncovered GNP surface was saturated with BSA. In detail, the colloidal solution of GNPs (1 mL) was added with 5 µL of a 1 $mg{\cdot}mL^{-1}$ solution of SpA in PB, incubated for 30 min at 37 °C, subsequently added with 100 µL of 1% w/v solution of BSA in borate buffer 20 mM pH 7.4, then incubated for 10 min at 37 °C and finally purified and concentrated by three repeated centrifugation (18,500*g*, 10 min, 25 °C).

2.6 Model FRET-based quenching assay

Non-competitive quenching experiments were carried out in a 96-well micro-titration plate. In each well, 100 µL of $CNNP^{Lys}$–IgG solution (0.1 $mg{\cdot}L^{-1}$) was mixed with 100 µL of GNP–SpA solution, with varying optical densities (OD = 0, 0.5, 1, and 2). After 30 min of incubation at room temperature the $CNNP^{Lys}$–IgG fluorescence was measured by means of the microplate fluorimeter (λexcitation = 340 ± 15 nm, λemission = 420 ± 25 nm). The Stern–Volmer plot was obtained from the PL intensities (I) and the PL signal in the absence of the quencher (I_0) recorded as a function of the quencher amount. As a control, the same experiment was carried out by mixing $CNNP^{Lys}$–IgG with GNPs saturated with BSA.

In the competitive quenching assay, 100 µL of CNNP–IgG solution 0.15 $mg{\cdot}mL^{-1}$ was added to 50 µL of free IgG with increasing concentration (0, 0.04, 0.4, 1, 4, 10, and 40 nM), and incubated for 10 min at room temperature. Then 50 µL of the GNP–SpA solution (OD = 2) was added. After 30 min incubation at room temperature, the fluorescence was measured as described above and plotted towards IgG concentration.

3 Results and discussion

3.1 Preparation of the amine-rich CNNPs

As widely reported, blue fluorescent CNNPs can be obtained from the thermal condensation of nitrogen-rich organic precursors such as urea—able to polymerize in condensed structures—possibly combined with an additional source of carbon and nitrogen (i.e. citrate, tartaric acid and glycine) [28, 29, 49]. These materials typically show pendant hydrophilic groups, which guarantee high water solubility and which have been exploited for sensing [2, 35]. Indeed, the complexation of metal ions with the superficial polar moieties modulated the material fluorescence and enabled the sensitive detection of the metal through measuring the CNNP fluorescence.

Initially, we prepared fluorescent CNNPs from urea and citrate as the precursors ($CNNP^{Cit}$), according to the protocol reported in [33], to employ them as the signal reporter for the development of bioanalytical methods based on the specific molecular recognition mechanism. Nevertheless, the conjugation of the $CNNP^{Cit}$ material to model bioligands (e.g. proteins), through different conjugation approaches was unsatisfactory. Specifically, hypothetic reactive carboxy- and amino-groups were exploited for covalently linking $CNNP^{Cit}$ to a model protein (BSA): Hence $CNNP^{Cit}$ was reacted with BSA using the EDC/NHS [50] and the glutaraldehyde [50, 51] methods, respectively. Both attempts failed, suggesting that neither carboxy- nor amino-groups were available for the conjugation to the protein. Likely, the functionalities, though existing, were insufficient or unavailable for enabling efficient bioconjugation. Therefore, we prepared new CNNPs by the one-pot, solid state, thermal induced condensation of urea and lysine. U is an ideal "conjugated polymer"-forming monomer due to its low cost, high nitrogen content and because it triggers the condensation reaction at relatively low temperature. In addition, a remarkable evolution of NH_3 gas arising from the decomposition of U near 180 °C, increased the pressure in the sealed reactor and ultimately accelerated the reaction rate [28]. Lys was chosen as the co-substrate with the aim to provide the final material with a high amount of free primary amino groups, suitable for the subsequent conjugation to biomolecules.

Optimal synthetic conditions for obtaining stable, water-soluble and high fluorescent CNNPs were defined by synthesizing eight CN-nanomaterials and comparing their optical properties, their hydrophilicity and the pH of their aqueous suspension. Accordingly, the U:Lys molar ratio was varied from 1 to 12 and the reaction time from 2 to 16 h. The prepared materials were screened by fluorescence spectroscopy to identify conditions providing higher PL. The hydrophilicity was estimated as the amount of raw products that freely dissolved in water by sonication (Fig. 1 and Table S1 in the Electronic Supplementary Material (ESM)). Noteworthily, the fraction

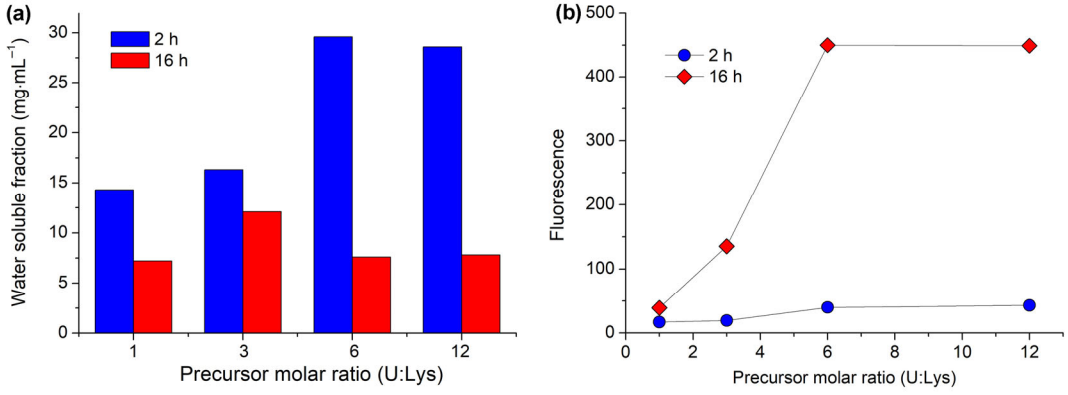

Figure 1 (a) Fraction of CN dissolved in water by sonication (undissolved matter was eliminated by 0.45 μm filtration) for different precursor ratios and heating time. (b) PL intensity (λexcitation = 340 nm) at maximum of emission for CNNPs as a function of the U:Lys molar ratios (heating time 2 and 16 h).

of the material that freely dissolved in water provided clear yellowish suspensions, stable for weeks without any flocculation.

All of the lysine-based CNNPs exhibited alkaline pH, ranging between 9 and 11, independently on the precursor ratio and heating time (Table S1 in the ESM). Conversely, CNNP^{Cit} showed acidic pH (ca. 6). The alkaline pH of lysine-based CNNPs was a reasonable indication of the presence of available amino-groups in these materials.

The fraction that dissolved in water was higher in the case of materials obtained after 2 h of heating compared to those obtained by prolonged thermal treatment (Fig. 1(a)). This evidence is coherent with the increasing condensation of the building blocks due to a longer thermal treatment, which gives more rigid and less hydrophilic structures. For materials obtained by 2 h heating time, the higher the precursor ratio, the higher the hydrophilicity of the CNNPs, while for the materials obtained by 16 h heating time, the hydrophilicity was less affected by the U fraction. The photoluminescence increased with the U amount until the 6:1 U:Lys ratio and then reached a plateau. However, the most relevant increase in PL emission (of almost one order of magnitude) was observed with increasing the heating time (Fig. 1(b)). Reasonably the condensed products obtained by prolonged heating had a more rigid structure. Based on PL and hydrophilicity, the CNNP material prepared from 6:1 precursor ratio and 16 h heating treatment (CNNP^{Lys}) was chosen for further experiments.

It should be noted that the thermally induced modification of pure precursors, using the same reaction conditions, resulted in soluble products that did not exhibit any fluorescence. U turned into a white powder because of the heating treatment with condensation and evolution of ammonia. On the contrary, Lys remained apparently unchanged by the thermal treatment as no weight loss and no change of the IR spectrum were observed. Just, the original white powder turned into pale yellow (see Fig. S1 in the ESM).

3.2 Characterization of the amine-rich CNNPs

ATR/FT-IR spectra were recorded to gain further insights into the local structure and the nature of the surface functional groups of CNNP^{Lys}. Most of the peaks were located at different frequencies when compared to the two precursors (pure U and Lys, both before and after the thermal treatment, Fig. S2 in the ESM), indicating the formation of new species with modified structures. Nevertheless, the shape of the whole CNNP^{Lys} fingerprint region (1,100–400 cm^{-1}) was largely similar to that of urea, indicating a common chemical structure. Figure 2 shows also the IR spectra of other CNNP materials, i.e. one obtained from a different precursor ratio (12:1 instead of 6.1) and another obtained by a shorter heating time (2 h). All spectra confirmed the presence of hydrophilic moieties, e.g. amino, hydroxyl and carboxylic groups, responsible for the water

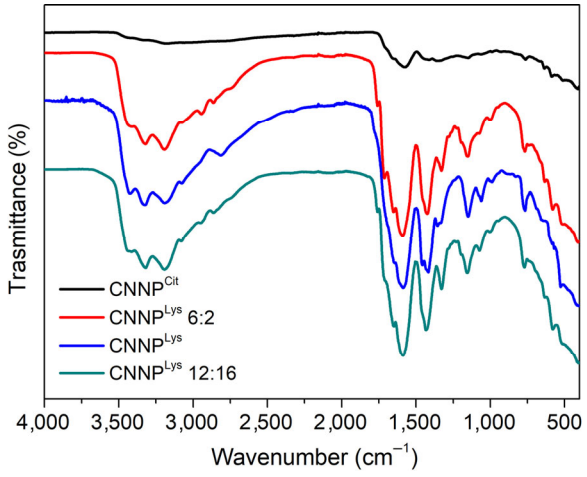

Figure 2 ATR/FT-IR spectra of CNNP^{Cit} and CNNP^{Lys} obtained from different precursor ratios/heating time, namely (6:1)/2 h (CNNP^{Lys} 6:2), (6:1)/16 h (CNNP^{Lys}) and (12:1)/16 h (CNNP^{Lys} 12:16).

solubility of CNNPs. The functionalities were respectively identified by the stretching vibrations peaks centered at 3,430, 3,330, 3,200 and 1,710 cm^{-1} [22, 26, 33]. Differently from CNNP^{Cit}, the new materials synthesized from lysine were rich in amino groups (Fig. 2). Several absorption bands were observed from 1,100 to 1,760 cm^{-1} in the CNNP^{Lys} spectrum. The bands located at 1,100–1,200 and 1,330 cm^{-1} were related to the progressive structure condensation. Accordingly, these were absent in the pristine U and moderately intense in the heated U (Fig. S2 in the ESM).

Bands between 1,100 and 1,330 cm^{-1}, together with the peak at 1,415 cm^{-1}, corresponded to the vibration modes of C–N (secondary and tertiary amines) and C=N, respectively, typical of aromatic heterocycles [14, 33, 39]. The bands at 1,600 and 1,655 cm^{-1} were ascribed to C=N and amidic C=O stretching [26, 29], respectively. The IR spectra of all CNNP materials prepared from Lys suggested that their chemical structure was different to that of bulky, poorly hydrophilic, polymeric carbon nitride [27, 35, 39]. The IR spectrum of bulky g-C_3N_4 usually shows several peaks in the 1,200–1,700 cm^{-1} region that are characteristic of the triazine ring system. In our materials, we observed absorptions in a narrower range (~ 1,400–1,700 cm^{-1}). Furthermore, the sharp peak at 800–815 cm^{-1} generally ascribed to the triazine/heptazine ring structures in bulky g-C_3N_4, was remarkably redshifted in the new CNNP materials, indicating smaller triazine domains. Instead, the IR spectrum of the CNNP^{Lys} was similar to those of carbon nitride nanoparticles previously reported, suggesting the nanoparticle nature of the new material [29, 33].

The measured N/C molar ratio of CNNP^{Lys} was 1.25. This value

is remarkably higher compared to that of nitrogen-rich carbon nanoparticles with similar features (N/C = 0.6–0.7 [26, 29, 33]). The higher nitrogen content was likely due to the N-rich co-precursor used. In addition, it strengthened the hypothesis of the existence of primary amino groups derived from the Lys side chain, not involved in the condensation process. This result also confirmed that the CNNP structure was different from that of bulky g-C_3N_4, which is characterized by an even higher N/C ratio (1.33) [27].

According to HR-TEM micrography, the new materials were formed by nanoparticles whose size increased with the reaction time (see Fig. S3 in the ESM). The $CNNP^{Lys}$, appeared roughly spherical in shape and approximately 150 nm in size (Fig. 3(a)). DLS measurement also confirmed estimation of nanoparticles size. $CNNP^{Lys}$ showed a slightly monomodal size distribution centered at ca. 110 nm (Fig. 3(b)). A minor fraction of particles with larger size (250–500 nm) was identified, too.

The optical properties of the $CNNP^{Lys}$ were investigated through UV–Vis and steady-state fluorescence emission spectroscopy. The absorption tails into the visible region was responsible for the yellowish color of the $CNNP^{Lys}$ solution. The UV–Vis absorption spectrum showed a broad band centered at 290 nm with a tail at 350–450 nm (Fig. 4(a)), besides the main absorption band centered below 220 nm. The absorption band at 290 nm was ascribed to π–π^* electronic transitions of heterocyclic conjugated systems, typically present in carbon nitrides, while the absorption shoulder at 310–320 nm presumably corresponded to the n–π^* transitions involving lone pairs in N=C and C=O moieties [26, 27, 29]. However, the absorption bands were shifted with respect to those reported in literature for g-C_3N_4 nanomaterials [27, 39], indicating again a different structure. Conversely, the weak characteristic peak at 320–340 nm, ascribed to the semiconducting bang gap adsorption of g-C_3N_4 [26, 39] is clearly visible.

The $CNNP^{Lys}$ showed a bright blue fluorescence emission under UV irradiation (Fig. 4(a) inset). Figure 4(b) shows the spectrofluorometric properties of $CNNP^{Lys}$ (excitation range 330–410 nm). The fluorescence profile evidenced a negative Stokes shift when the material was excited at increasing wavelengths (see inset Fig. 4(b)). This behavior suggested a distribution of excited electronic states, possibly related to the heterogeneity of the particle sizes. The PL profile under 330 nm excitation revealed a residual contribution of the DCM-partitioned fraction, which owned high fluorescence emission but scarce availability of free amino-groups. To avoid interference from this fraction, the following experiments were carried out by exciting the fluorescence at 340 nm and measuring the emission at 410 nm. The relative QY was estimated through the comparison of the fluorescence of the $CNNP^{Lys}$ with that of a reference solution of quinine in 1 N H_2SO_4, according to Eq. (1)

$$QY = \frac{I}{I_R} \times \frac{A_R}{A} \times \frac{\eta^2}{\eta_R^2} \times QY_R \quad (1)$$

where I_R and I are the areas under the PL curve of quinine and $CNNP^{Lys}$, respectively; A_R and A are the absorbance values for quinine and $CNNP^{Lys}$ at 340 nm, and η^2/η_R^2 is the quadratic ratio of the refractive index of 1 N H_2SO_4 (η_R = 1.3) and water (η = 1.33) [52]. The absorbance of the solutions was kept lower than 0.05 UA. The reference value for quinine quantum yield (QY_R) at 340 nm was 0.55 [53].

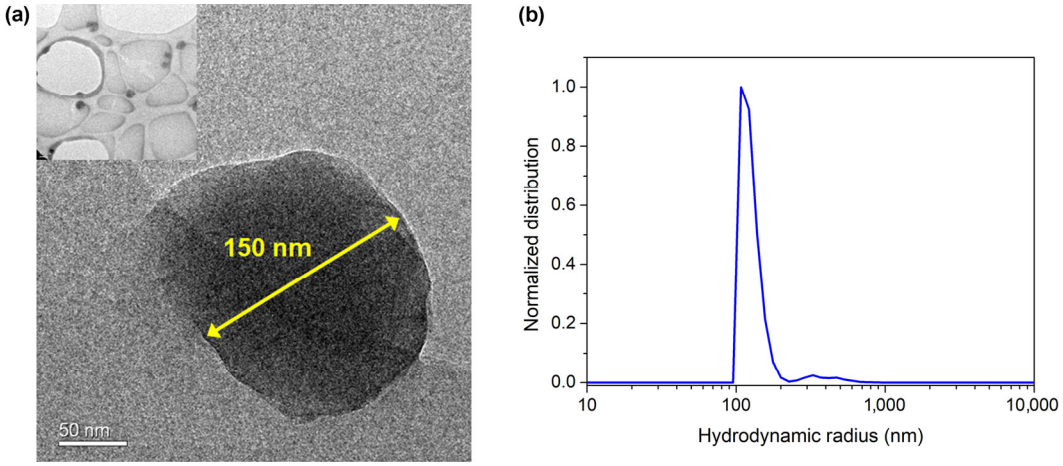

Figure 3 (a) HR-TEM of $CNNP^{Lys}$ at different magnifications. (b) Number averaged distribution of $CNNP^{Lys}$ in water as measured by DLS.

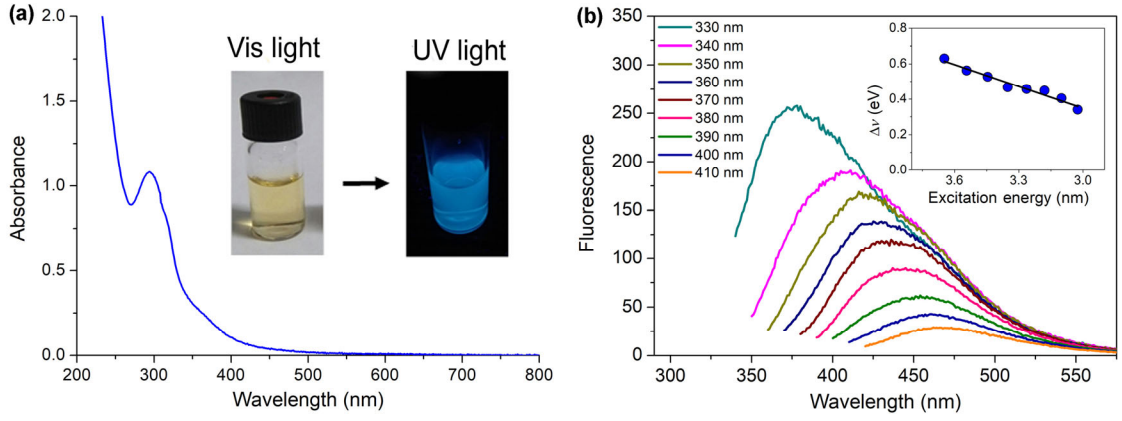

Figure 4 (a) UV–Vis absorption spectrum of $CNNP^{Lys}$. Inset: $CNNP^{Lys}$ under ambient light and under UV irradiation (365 nm). (b) Fluorescence emission spectra of $CNNP^{Lys}$ excited at different λ (from 330 to 410 nm, in 10 nm increments). The $CNNP^{Lys}$ concentration was 0.4 mg·mL^{-1}. Inset: Stokes shift as a function of the excitation energy.

The relative QYs for CNNP^{Lys} was then calculated as 24.0%. Besides carbon nitride QDs and nanosheets reported in [28, 41], which showed QY close to 50%, the value for CNNP^{Lys} is similar or slightly higher compared to other CN-based nanomaterials [22, 27, 29].

3.3 Covalent conjugation to model proteins

The feasibility of the conjugation between CNNP^{Lys} and proteins through covalent linking was explored using BSA as a model protein and glutaraldehyde as the cross-linker [51]. Glutaraldehyde acts as a homo-bifunctional linker between two primary amino-groups. Therefore, the formation of a conjugate between CNNP^{Lys} and BSA was considered as a proof of the availability of free amino groups from the fluorescent nanoparticles. CNNP^{Cit} was submitted to the same conjugation protocol, and to the EDC/NHS linking protocol. After the conjugation process, the conjugated and unconjugated species were separated by SEC (Fig. 5). The eluted fractions were stained with the Bradford reagent [46] to reveal those containing the protein. At the same time, the fluorescence emission of the eluted fractions was recorded to highlight the presence of the CNNPs. The concurrent detection of the protein and the CNNPs was reasonably assumed as an index of the successful CNNP–BSA conjugation.

The conjugation to BSA occurred successfully for the CNNP^{Lys} (Fig. 5(a)) while no conjugation was observed for the CNNP^{Cit} (by both glutaraldehyde and EDC/NHS conjugation approaches), as demonstrated by the absence of overlap between the signal related to the protein and that of the fluorescent CNNPs (as an example, Fig. 5(b) shows the product obtained by using glutaraldehyde as the cross-linker). This result was in agreement with the characterization described above and confirmed the presence of freely available amino groups in the CNNP^{Lys} material. Moreover, the functional groups were reactive and allowed for the direct attachment of biomolecules without requiring any additional modification.

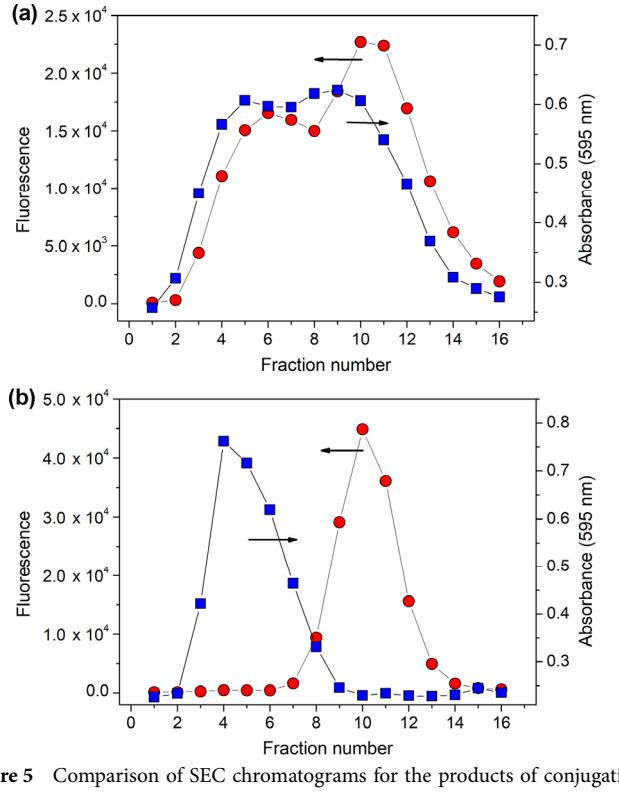

Figure 5 Comparison of SEC chromatograms for the products of conjugation between BSA and CNNP^{Lys} (a) and CNNP^{Cit} (b) via the glutaraldehyde cross-linking. The red circles represent the fluorescence signal of the eluted fractions (λ_{exc} = 340 nm, λ_{em} = 420 nm), while the blue squares represent the profile of protein concentration as measured by the absorbance at 595 nm after staining with Brilliant Blue Comassie.

3.4 FRET-based quenching assay

The potential use of the novel CNNP^{Lys} as a convenient fluorescence probe for biosensing was demonstrated in a one-step model assay based on the fluorescence quenching principle. GNPs characterized by a surface plasmon resonance (SPR) band centered at 525 nm were used for quenching the CNNP^{Lys} photoluminescence through the FRET phenomenon.

In order to achieve a specific recognition-related signal, the CNNP^{Lys} and the GNPs were conjugated with a ligand and a receptor, respectively. Specifically, CNNP^{Lys} were covalently linked to rabbit immunoglobulins (CNNP^{Lys}–IgG) and GNPs were adsorbed with Staphylococcal protein A (GNP–SpA). The CNNP^{Lys}–IgG probe was prepared as described above using IgG instead of BSA, and again confirming the successful conjugation by SEC. The GNP–SpA quencher was obtained via passive adsorption of SpA onto GNPs and the conjugation was confirmed by the shift of the maximum of the GNP SPR band (Fig. S4 in the ESM) [54].

The principle of the fluorescence quenching assay exploiting CNNP^{Lys} as the fluorescent probe is shown in Scheme 1. The 340 nm irradiation excited the fluorescent probe, which relaxed radiatively providing a signal at 420 nm. Upon mixing CNNP^{Lys}–IgG and GNP–SpA, the 420 nm emission from CNNP^{Lys}–IgG was absorbed by the quencher through a resonant energy transfer, because the fluorescent probe and the quencher were kept at a sufficient close proximity by the SpA–IgG complex formation.

Free IgG added in the system inhibited the binding of CNNP^{Lys}-labelled IgG to GNP-SpA, with a consequent recovery of the fluorescent signal.

The exciting wavelength was absorbed partially by the quencher, since the molar extinction coefficient of GNPs is not negligible at 340 nm (Fig. S4 in the ESM). Therefore, also the inner filter effect (IFE) contributed to the decrease of the signal at 420 nm. The assay response was studied by plotting the CNNP fluorescence as a function of the quencher (GNP–SpA) amount. The assay was carried out by mixing the CNNP^{Lys}-IgG probe to GNPs linked to the specific recognition element (GNP–SpA) and to bare GNPs (that is GNPs saturated with BSA), as a control. The signal measured at 420 nm

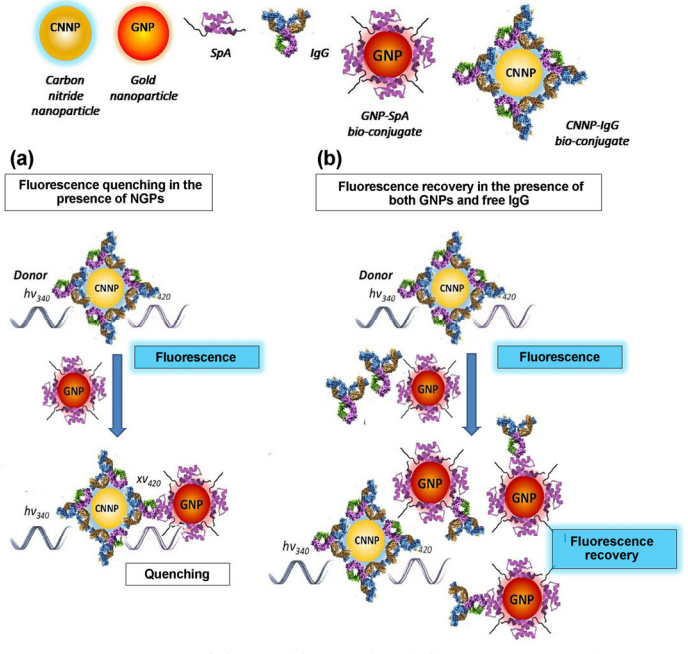

Scheme 1 Principles of the model FRET-based fluorescence quenching assay: (a) the specific binding between the ligand and the receptor results in conditions suitable for the energy transfer and the CNNP emission is quenched. (b) Addition of free ligand (IgG) inhibits the binding of the fluorescent labelled ligand to the receptor and the probe emission is turned on.

decreased as a function of increasing the quencher amount (Fig. 6(a), where I and I_0 are the fluorescence signals in the presence and absence of the quencher, respectively). The exciting wavelength was absorbed partially by the quencher, since the molar extinction coefficient of GNPs is not negligible at 340 nm (Fig. S4 in the ESM). The contribution of the non-specific quenching due to the inner filter effect was quantified from the bare GNPs control. The difference between the decreasing rate measured using GNP–SpA or bare GNPs was assumed as an estimation of the quenching effect related to the FRET mechanism. In turn, the FRET quenching occurred because of the formation of the SpA-IgG specific binding. The resulting Stern–Volmer plots (Fig. 6(a)) show, in both cases, a linear trend with a slope that is double for the GNP–SpA (specific quenching) than for bare GNPs (IFE).

The contribution of the specific recognition was further confirmed by introducing unlabeled human IgG into the system. Upon addition of human IgG, the specific binding between GNP–SpA and CNNP^{Lys}–IgG was inhibited [56]. As a result, the CNNP fluorescence was recovered (Fig. 6(b)). The CNNP^{Lys} fluorescence increased as a function of the human IgG concentration in a wide range of concentration (0.1–10 nm), and with limit of detection lower than the nanomolar level, highlighting that CNNP^{Lys} was an efficient and sensitive probe to develop a fluorescence quenching biosensor. The limit of detection (LOD) was estimated as the blank + 3 sd, and was 0.08 nM, which is far lower than the typical concentration of IgG in human serum (65–70 μM [57]). Compared to previously reported one-step assays for detecting IgG based on the fluorescence quenching mechanism, the CNNP^{Lys}-probe enabled generally higher sensitivity (Table 1).

The LOD was two/three orders of magnitude lower, except for the work of Zhang et al. who reported an ultra-high sensitivity with LOD down to 0.005 nM [60].

As albumin is the most abundant serum protein, we verified the effect of the presence of this protein as a potential interfering substance from real samples. No fluorescence signal was registered for human albumin concentrations up to 1 μM, confirming the specific recognition mechanism of the assay.

4 Conclusions

A one-pot and low temperature solid-phase method was exploited for preparing fluorescent and soluble CNNPs with specific desired surface functionalities. PL yield and availability of surface functional groups were optimized by acting both on the chemical nature of the precursors and on the reaction time. Amino-groups available for the covalent linking to proteins were obtained by using lysine as the co-precursor, mixed to urea. Compared to other CNNPs previously reported, the as-prepared materials showed definitely higher availability of functional groups suitable for their covalent binding to bioligands.

The CNNP^{Lys} allowed for preparing a protein conjugate, which was used as a fluorescent probe in a FRET quenching assay, with functionalized GNPs as the quencher. This system resulted in a very sensitive tool for the detection of human immunoglobulins G. With respect to inorganic quantum dots, the material here proposed is highly water compatible and does not need neither post-synthesis functionalization nor covering with hydrophilic films. In addition, these CNNPs maintained unvaried PL properties after covalent binding to proteins. These aspects are crucial for the development of new bioanalytical methods and especially for biosensing applications. The synthetic approach developed in this work can be generalized to design new CNNP-based materials with tailored surface functionalization (i.e. –COOH, –OH, –PhOH, –SH).

Acknowledgements

The financial support from project Ricerca Locale-Torino University is gratefully acknowledged.

Electronic Supplementary Material: Supplementary material (further details on the materials synthesized at different U:Lys molar ratio and heating time, IR spectra of the precursors before and after the thermal treatment, HR-TEM on CNNP^{Lys} 6:2, UV–Vis spectra of GNPs before and after conjugation with SpA) is available in the

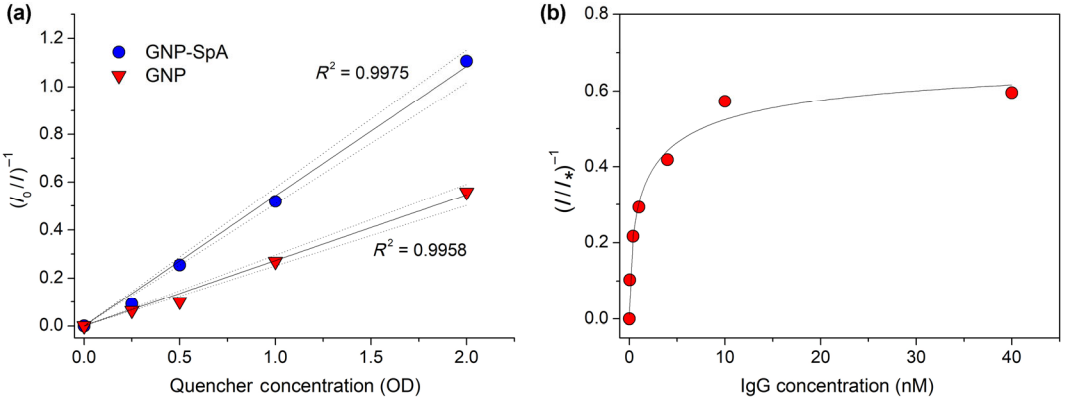

Figure 6 FRET-based quenching assay. (a) Stern–Volmer plot for CNNP^{Lys} fluorescence quenching as a function of the quencher amount for GNP–SpA (blue circles) and bare GNPs (red triangles). I_0 and I are the fluorescence intensities without and with the quencher, respectively. (b) Recovery of the fluorescence signal as a function of the human IgG concentration with a quencher concentration equal to 2 OD (I_* and I are the fluorescence intensities in the absence of and at increasing IgG concentration, respectively). Experimental data were fitted by a nonlinear regression analysis using the four-parameter logistic equation [55].

Table 1 Analytical figures of merits of one-step immunoassay for measuring IgG based on fluorescent quenching

Probe/quencher	Method	Limit of detection (nm)	Working range (nm)	Sample	Ref.
BODIPY dye selectively binding IgG/IgG	Inhibition assay	nd	22,000–83,000	Serum	[58]
Fluorescein-labelled IgG/graphene oxide nanosheets	Ratiometric assay	4.67	nd	Buffer	[59]
Fluorescent polymer (poly[2,5-di(propyloxysulfonate)-1,4-phenylene-ethynylene-9,10-anthrylene)/IgG	Inhibition assay	0.005	0.033–6.67	Buffer	[60]
Atto655-labeled binding peptide/complementary quenching peptide	Ratiometric assay	nd	50–7,500	Buffer	[61]
CNNP^{Lys}–IgG/GNP–SpA	Ratiometric assay	0.08	0.1–10	Buffer	This work

online version of this article at https://doi.org/10.1007/s12274-019-2449-x.

References

[1] Sharma, A.; Khan, R.; Catanante, G.; Sherazi, T. A.; Bhand, S.; Hayat, A.; Marty, J. L. Designed strategies for fluorescence-based biosensors for the detection of mycotoxins. *Toxins* **2018**, *10*, 197.

[2] Feng, X. L.; Liu, L. B.; Wang, S.; Zhu, D. B. Water-soluble fluorescent conjugated polymers and their interactions with biomacromolecules for sensitive biosensors. *Chem. Soc. Rev.* **2010**, *39*, 2411–2419.

[3] Liu, G. D.; Wang, J.; Kim, J.; Jan, M. R.; Collins, G. E. Electrochemical coding for multiplexed immunoassays of proteins. *Anal. Chem.* **2004**, *76*, 7126–7130.

[4] Martynenko, I. V.; Litvin, A. P.; Purcell-Milton, F.; Baranov, A. V.; Fedorov, A. V.; Gun'ko, Y. K. Application of semiconductor quantum dots in bioimaging and biosensing. *J. Mater. Chem. B* **2017**, *5*, 6701–6727.

[5] Derfus, A. M.; Chan, W. C. W.; Bhatia, S. N. Probing the cytotoxicity of semiconductor quantum dots. *Nano Lett.* **2004**, *4*, 11–18.

[6] Wolfbeis, O. S. An overview of nanoparticles commonly used in fluorescent bioimaging. *Chem. Soc. Rev.* **2015**, *44*, 4743–4768.

[7] Goftman, V. V.; Aubert, T.; Ginste, D. V.; Van Deun, R.; Beloglazova, N. V.; Hens, Z.; De Saeger, S.; Goryacheva, I. Y. Synthesis, modification, bioconjugation of silica coated fluorescent quantum dots and their application for mycotoxin detection. *Biosens. Bioelectron.* **2016**, *79*, 476–481.

[8] Speranskaya, E. S.; Beloglazova, N. V.; Lenain, P.; De Saeger, S.; Wang, Z. H.; Zhang, S. X.; Hens, Z.; Knopp, D.; Niessner, R.; Potapkin, D. V. et al. Polymer-coated fluorescent CdSe-based quantum dots for application in immunoassay. *Biosens. Bioelectron.* **2014**, *53*, 225–231.

[9] Baker, S. N.; Baker, G. A. Luminescent carbon nanodots: Emergent nanolights. *Angew. Chem., Int. Ed.* **2010**, *49*, 6726–6744.

[10] Luo, P. G.; Sahu, S.; Yang, S. T.; Sonkar, S. K.; Wang, J. P.; Wang, H. F.; LeCroy, G. E.; Cao, L.; Sun, Y. P. Carbon "quantum" dots for optical bioimaging. *J. Mater. Chem. B* **2013**, *1*, 2116–2127.

[11] Wen, J.; Xu, Y. Q.; Li, H. J.; Lu, A. P.; Sun, S. G. Recent applications of carbon nanomaterials in fluorescence biosensing and bioimaging. *Chem. Commun.* **2015**, *51*, 11346–11358.

[12] Bhunia, S. K.; Saha, A.; Maity, A. R.; Ray, S. C.; Jana, N. R. Carbon nanoparticle-based fluorescent bioimaging probes. *Sci. Rep.* **2013**, *3*, 1473.

[13] Esteves da Silva, J. C. G.; Gonçalves, H. M. R. Analytical and bioanalytical applications of carbon dots. *TrAC Trends Anal. Chem.* **2011**, *30*, 1327–1336.

[14] Barman, S.; Sadhukhan, M. Facile bulk production of highly blue fluorescent graphitic carbon nitride quantum dots and their application as highly selective and sensitive sensors for the detection of mercuric and iodide ions in aqueous media. *J. Mater. Chem.* **2012**, *22*, 21832–21837.

[15] Li, Q.; Ohulchanskyy, T. Y.; Liu, R. L.; Koynov, K.; Wu, D. Q.; Best, A.; Kumar, R.; Bonoiu, A.; Prasad, P. N. Photoluminescent carbon dots as biocompatible nanoprobes for targeting cancer cells *in vitro*. *J. Phys. Chem. C* **2010**, *114*, 12062–12068.

[16] Chen, B. S.; Li, F. M.; Li, S. X.; Weng, W.; Guo, H. X.; Guo, T.; Zhang, X. Y.; Chen, Y. B.; Huang, T. T.; Hong, X. L. et al. Large scale synthesis of photoluminescent carbon nanodots and their application for bioimaging. *Nanoscale* **2013**, *5*, 1967–1971.

[17] Zuo, J.; Jiang, T.; Zhao, X. J.; Xiong, X. H.; Xiao, S. J.; Zhu, Z. Q. Preparation and application of fluorescent carbon dots. *J. Nanomater.* **2015**, *2015*, 787862.

[18] Cao, L.; Meziani, M. J.; Sahu, S.; Sun, Y. P. Photoluminescence properties of graphene versus other carbon nanomaterials. *Acc. Chem. Res.* **2013**, *46*, 171–180.

[19] Wu, P.; Yan, X. P. Doped quantum dots for chemo/biosensing and bioimaging. *Chem. Soc. Rev.* **2013**, *42*, 5489–5521.

[20] Chandra, S.; Patra, P.; Pathan, S. H.; Roy, S.; Mitra, S.; Layek, A.; Bhar, R.; Pramanik, P.; Goswami, A. Luminescent S-doped carbon dots: An emergent architecture for multimodal applications. *J. Mater. Chem. B* **2013**, *1*, 2375–2382.

[21] Tabaraki, R.; Abdi, O.; Yousefipour, S. Green and selective fluorescent sensor for detection of Sn (IV) and Mo (VI) based on boron and nitrogen-co-doped carbon dots. *J. Fluoresc.* **2017**, *27*, 651–657.

[22] Lu, Y. C.; Chen, J.; Wang, A. J.; Bao, N.; Feng, J. J.; Wang, W. P.; Shao, L. X. Facile synthesis of oxygen and sulfur co-doped graphitic carbon nitride fluorescent quantum dots and their application for mercury(II) detection and bioimaging. *J. Mater. Chem. C* **2015**, *3*, 73–78.

[23] Tian, J. Q.; Liu, Q.; Asiri, A. M.; Al-Youbi, A. O.; Sun, X. P. Ultrathin graphitic carbon nitride nanosheet: A highly efficient fluorosensor for rapid, ultrasensitive detection of Cu^{2+}. *Anal. Chem.* **2013**, *85*, 5595–5599.

[24] Zhang, X. D.; Xie, X.; Wang, H.; Zhang, J. J.; Pan, B. C.; Xie, Y. Enhanced photoresponsive ultrathin graphitic-phase C_3N_4 nanosheets for bioimaging. *J. Am. Chem. Soc.* **2013**, *135*, 18–21.

[25] Wang, Q. B.; Wang, W.; Lei, J. P.; Xu, N.; Gao, F. L.; Ju, H. X. Fluorescence quenching of carbon nitride nanosheet through its interaction with DNA for versatile fluorescence sensing. *Anal. Chem.* **2013**, *85*, 12182–12188.

[26] Cao, X. T.; Ma, J.; Lin, Y. P.; Yao, B. X.; Li, F. M.; Weng, W.; Lin, X. C. A facile microwave-assisted fabrication of fluorescent carbon nitride quantum dots and their application in the detection of mercury ions. *Spectrochim. Acta Part A* **2015**, *151*, 875–880.

[27] Zhan, Y.; Liu, Z. M.; Liu, Q. Q.; Huang, D.; Wei, Y.; Hu, Y. C.; Lian, X. J.; Hu, C. F. A facile and one-pot synthesis of fluorescent graphitic carbon nitride quantum dots for bio-imaging applications. *New J. Chem.* **2017**, *41*, 3930–3938.

[28] Zhou, J.; Yang, Y.; Zhang, C. Y. A low-temperature solid-phase method to synthesize highly fluorescent carbon nitride dots with tunable emission. *Chem. Commun.* **2013**, *49*, 8605–8607.

[29] Guo, J. Q.; Lin, Y. P.; Huang, H.; Zhang, S. C.; Huang, T. T.; Weng, W. One-pot fabrication of fluorescent carbon nitride nanoparticles with high crystallinity as a highly selective and sensitive sensor for free chlorine. *Sens. Actuators B* **2017**, *244*, 965–971.

[30] Shen, L. M.; Zhang, L. P.; Chen, M. L.; Chen, X. W.; Wang, J. H. The production of pH-sensitive photoluminescent carbon nanoparticles by the carbonization of polyethylenimine and their use for bioimaging. *Carbon* **2013**, *55*, 343–349.

[31] Cao, S. W.; Low, J. X.; Yu, J. G.; Jaroniec, M. Polymeric photocatalysts based on graphitic carbon nitride. *Adv. Mater.* **2015**, *27*, 2150–2176.

[32] Zhang, Y. J.; Mori, T.; Ye, J. H. Polymeric carbon nitrides: Semiconducting properties and emerging applications in photocatalysis and photoelectrochemical energy conversion. *Sci. Adv. Mater.* **2012**, *4*, 282–291.

[33] Ren, X. L.; Meng, X. W.; Ren, J.; Tang, F. Q. Graphitic carbon nitride nanosheets with tunable optical properties and their superoxide dismutase mimetic ability. *RSC Adv.* **2016**, *6*, 92839–92844.

[34] Capilli, G.; Costamagna, M.; Sordello, F.; Minero, C. Synthesis, characterization and photocatalytic performance of p-type carbon nitride. *Appl. Catal. B: Environ.* **2019**, *242*, 121–131.

[35] Shiravand, G.; Badiei, A.; Ziarani, G. M. Carboxyl-rich g-C_3N_4 nanoparticles: Synthesis, characterization and their application for selective fluorescence sensing of Hg^{2+} and Fe^{3+} in aqueous media. *Sens. Actuators B* **2017**, *242*, 244–252.

[36] Liu, S.; Tian, J. Q.; Wang, L.; Luo, Y. L.; Sun, X. P. A general strategy for the production of photoluminescent carbon nitride dots from organic amines and their application as novel peroxidase-like catalysts for colorimetric detection of H_2O_2 and glucose. *RSC Adv.* **2012**, *2*, 411–413.

[37] Wang, S.; Liu, R. Q.; Li, C. C. Highly selective and sensitive detection of Hg^{2+} based on Förster resonance energy transfer between CdSe quantum dots and g-C_3N_4 nanosheets. *Nanoscale Res. Lett.* **2018**, *13*, 235.

[38] Han, J.; Zou, H. Y.; Gao, M. X.; Huang, C. Z. A graphitic carbon nitride based fluorescence resonance energy transfer detection of riboflavin. *Talanta* **2016**, *148*, 279–284.

[39] Wang, Y. P.; Wang, J. S.; Ma, P. P.; Yao, H. C.; Zhang, L.; Li, Z. J. Synthesis of fluorescent polymeric carbon nitride quantum dots in molten salts for security inks. *New J. Chem.* **2017**, *41*, 14918–14923.

[40] Lazauskas, A.; Baltrusaitis, J.; Puodžiukynas, L.; Andrulevičius, M.; Bagdžiūnas, G.; Volyniuk, D.; Meškinis, Š.; Niaura, G.; Tamulevičius, T.; Jankauskaitė, V. Characterization of urea derived polymeric carbon nitride and resultant thermally vacuum deposited amorphous thin films: Structural, chemical and photophysical properties. *Carbon* **2016**, *107*, 415–425.

[41] Zhuang, Q. F.; Sun, L. M.; Ni, Y. N. One-step synthesis of graphitic carbon nitride nanosheets with the help of melamine and its application for fluorescence detection of mercuric ions. *Talanta* **2017**, *164*, 458–462.

[42] Bai, X. J.; Yan, S. C.; Wang, J. J.; Wang, L.; Jiang, W. J.; Wu, S. L.; Sun, C. P.; Zhu, Y. F. A simple and efficient strategy for the synthesis of a chemically tailored g-C_3N_4 material. *J. Mater. Chem. A* **2014**, *2*, 17521–17529.

[43] Hou, Y. X.; Lu, Q. J.; Deng, J. H.; Li, H. T.; Zhang, Y. Y. One-pot electrochemical synthesis of functionalized fluorescent carbon dots and their selective sensing for mercury ion. *Anal. Chim. Acta* **2015**, *866*, 69–74.

[44] Förster, T. Zwischenmolekulare energiewanderung und fluoreszenz. *Ann. Phys.* **1948**, *437*, 55–75.

[45] Minella, M.; Demontis, M.; Sarro, M.; Sordello, F.; Calza, P.; Minero, C. Photochemical stability and reactivity of graphene oxide. *J. Mater. Sci.* **2015**, *50*, 2399–2409.
[46] Bradford, M. M. A rapid and sensitive method for the quantitation of microgram quantities of protein utilizing the principle of protein-dye binding. *Anal. Biochem.* **1976**, *72*, 248–254.
[47] Anfossi, L.; Di Nardo, F.; Profiti, M.; Nogarol, C.; Cavalera, S.; Baggiani, C.; Giovannoli, C.; Spano, G.; Ferroglio, E.; Mignone, W. et al. A versatile and sensitive lateral flow immunoassay for the rapid diagnosis of visceral leishmaniasis. *Anal. Bioanal. Chem.* **2018**, *410*, 4123–4134.
[48] Turkevich, J.; Stevenson, P. C.; Hillier, J. A study of the nucleation and growth processes in the synthesis of colloidal gold. *Discuss. Faraday Soc.* **1951**, *11*, 55–75.
[49] Li, L. B.; Li, L.; Wang, C.; Liu, K. Y.; Zhu, R. H.; Qiang, H.; Lin, Y. Q. Synthesis of nitrogen-doped and amino acid-functionalized graphene quantum dots from glycine, and their application to the fluorometric determination of ferric ion. *Microchim. Acta* **2015**, *182*, 763–770.
[50] Ghica, M. E.; Pauliukaite, R.; Fatibello-Filho, O.; Brett, C. M. A. Application of functionalised carbon nanotubes immobilised into chitosan films in amperometric enzyme biosensors. *Sens. Actuators B* **2009**, *142*, 308–315.
[51] Hermanson, G. T. *Bioconjugate Techniques*, 3rd ed.; Elsevier: Amsterdam, 2013.
[52] Lakowicz, J. R. *Principles of Fluorescence Spectroscopy*; Springer: New York, 1983.
[53] Brouwer, A. M. Standards for photoluminescence quantum yield measurements in solution (IUPAC Technical Report). *Pure Appl. Chem.* **2011**, *83*, 2213–2228.
[54] Jazayeri, M. H.; Amani, H.; Pourfatollah, A. A.; Pazoki-Toroudi, H.; Sedighimoghaddam, B. Various methods of gold nanoparticles (GNPs) conjugation to antibodies. *Sens. Bio-Sens. Res.* **2016**, *9*, 17–22.
[55] Dunn, J.; Wild, D. Calibration curve fitting. In *The Immunoassay Handbook: Theory and Applications of Ligand Binding, ELISA and Related Techniques*. Wild, D., Ed.; 4th ed. Elsevier: Amsterdam, 2013; pp 323–336.
[56] Zhao, D. H.; Swager, T. M. Sensory responses in solution vs solid state: A fluorescence quenching study of poly(iptycenebutadiynylene)s. *Macromolecules* **2005**, *38*, 9377–9384.
[57] De, M.; Rana, S.; Akpinar, H.; Miranda, O. R.; Arvizo, R. R.; Bunz, U. H. F.; Rotello, V. M. Sensing of proteins in human serum using conjugates of nanoparticles and green fluorescent protein. *Nat. Chem.* **2009**, *1*, 461–465.
[58] Vendrell, M.; Krishna, G. G.; Ghosh, K. K.; Zhai, D. T.; Lee, J. S.; Zhu, Q.; Yau, Y. H.; Shochat, S. G.; Kim, H.; Chung, J. et al. Solid-phase synthesis of BODIPY dyes and development of an immunoglobulin fluorescent sensor. *Chem. Commun.* **2011**, *47*, 8424–8426.
[59] Huang, A.; Li, W. W.; Shi, S.; Yao, T. M. Quantitative fluorescence quenching on antibody-conjugated graphene oxide as a platform for protein sensing. *Sci. Rep.* **2017**, *7*, 40772.
[60] Zhang, P.; Zhuo, S. J.; Sun, L. L.; Zhang, P.; Zhu, C. Q. Determination of gamma-globulin at nanogram levels by its quenching effect on the fluorescence of a red emitting conjugated polymer. *New J. Chem.* **2015**, *39*, 4551–4555.
[61] Okochi, M.; Sugita, T.; Tanaka, M.; Honda, H. A molecular peptide beacon for IgG detection. *RSC Adv.* **2015**, *5*, 91988–91992.